4
Novel NIR-II Emissive Cr(0) Complex Synthesis, TD-DFT and Biological Evaluation

Research Article based on this study:
Singh, T.; Yadav V.; Bhattachrayya, S., Chakraborty, S. NIR-II Emissive Cr(0) Complex: Synthesis, Structure, TD-DFT and Bioactivity. (Manuscript to be submitted).

4.1 Introduction

Resistance to antimicrobial drugs is one of the global concerns as it has hampered the global economy and civilization's health at a broader scale for a couple of decades. This dreaded trouble arises in human pathogens due to irrational and unbridled clinical usage of available antimicrobial agents and the haphazard intake of antibiotics in food and fodder industries.[286] These deranged situations bring in demand for the discovery and development of new therapeutic interventions to control the worldwide problem of antibiotic resistance. Drug-resistant bacteria are classified into several groups, but multidrug-resistant strains of pathogenic bacteria are the major cause of worldwide causality.[287] Drug-resistant report published in 2019 states that worldwide, 7.7 million individuals died in one year only because of bacterial infections. Interestingly, death due to bacterial infections falls on the second spot as compared to the first place taken by the heart disorder.[288-289] Although there are billions and billions of types of bacteria residing in the surroundings, only 33 predominately cause infections. Out of that, only a few bacteria, including *Escherichia coli*, *Staphylococcus aureus*, *Klebsiella pneumoniae*, *Streptococcus pneumoniae* and *Pseudomonas aeruginosa,* cause more than half of the infections[288,290]. So, in order to tackle this problem, we first need to develop new therapeutic interventions for these predominant bacteria.

In this context, medicinal inorganic chemistry offers an opportunity to discover new therapeutic agents.[291-294] In recent years, this field has been growing rapidly, and the role of transition metal complexes as therapeutic compounds is gaining increasing importance.[295] The possible formation of myriads of transition metal complexes with judicious choice of organic ligands and exploitation of the unique properties of metal-specific modes of action that are not available for organic antibiotics led to the design of new drugs for potential application in anti-bacterial and other diseases.[296-302] In particular transition metal complexes containing Schiff bases have garnered significant attention over the years largely because of their biological activities among various other applications.[303-316] However, most of the complexes are based on precious platinum group metals, which are expensive and potentially toxic.[317-321] In this regard, 3d transition metal complexes-based antibiotics are valuable alternatives because of their bio-compatibility, earth-abundance and cost-effectiveness.[322-325] There are several reports on the synthesis and biological evaluation based on first-row metal complexes. Recently, Giorgio and Angelo the group of developed manganese-based complexes and explored their activity in antimicrobial activity.[326]

Group VI metal chromium-based transition metal complexes are attractive alternatives in developing therapeutic agents because of their bio-compatibility and earth-abundance.[327] Study suggests that a 35µg dietary intake of chromium is necessary for humans to ensure the smooth functioning of the heart and brain; it is also essential for carbohydrate and lipid metabolism.[328] It has the unique feature of forming stable complexes with amino acids of

microbial cellular proteins. The toxicity of Cr complexes is governed by their oxidation number, the nature of binding species, and solubility. Cr (III) and Cr (0) complexes are rather low or non-toxic in comparison with carcinogenic and highly toxic Cr(VI) complexes.[329-331] Chromium Schiff base complexes have been explored as anti-inflammatory, antioxidant, anti-cancer, pesticidal, nematicidal, anti-fungal and anti-bacterial agents.[332-341] But reports based on 2-pyridylhydrazone derived low valent chromium complexes are rare in literature.[342]

4.2 Results & Discussion

This work presents a newly synthesized chromium-complex **Cr-1** and its potential biological application as an antimicrobial lead molecule. To deduce the antibacterial property of the complex of interest **Cr-1**, we first performed the *in vitro* agar diffusion test followed by *in silico* pharmacophore-guided therapeutic target screening through the rational approach of drug design and discovery. Interestingly, this newly synthesized chromium-complex **Cr-1** exhibits anti-bacterial activity against Gram-positive bacteria, including *B. subtilis* and *S. aureus*. Additionally, our *in-silico* pharmacophore-based drug discovery trajectory has demonstrated a rational mechanism of bactericidal actions for the synthesized chromium-complex **Cr-1**. Our results corroborate that this ligand moiety can bind at the active site of the AP endonuclease (endonuclease-IV), a major DNA repair enzyme in the cells. AP endonuclease protects bacteria, eukaryotes and even higher-order organisms from dsDNA break-induced cell death. The *in silico* and *in vitro* experimental outcomes and probable mode of action of chromium-complex **Cr-1** against Gram-positive bacterial pathogens are described herein. This comprehensive in silico and in vitro-based information deduced in the presented work would be impactful to precisely target the drug-resistant Gram-positive bacteria without affecting Gram-negative gut microbiota. This aforementioned chemically synthesized moiety will give us the foundation of antimicrobial development as a therapeutic lead in the future.

Primarily, the ligand synthesis was carried out according to the literature procedure by adding the ethanolic solution of 2-pyridyl hydrazine to the ethanolic solution of 2-bromobenzaldehyde dropwise, a catalytic amount of acetic acid was added, after which imine formation started immediately. The resulting solution was stirred for an hour at room temperature. Afterwards, the reaction was stopped, and the white precipitates thus obtained were collected and dried under a vacuum.[342] Afterwards, $Cr(CO)_6$ 73 mg (0.33 mmol) was added to the 25 mL Schlenk flask already charged with toluene solution of L 275 mg (1 mmol) inside the glove box. Schlenk was taken out of the glove box and heated to 130 °C over a pre-heated oil bath. Afterwards, the reaction was stopped and allowed to cool up to room temperature; the reddish-brown solution thus obtained was dried under vacuum and washed twice with pentane. Single crystals suitable for diffraction were obtained in saturated methanol solution using a slow evaporation technique. As per our expectation, an oxidatively added compound analogous to previously reported literature for a tungsten compound to generate a Cr(II) complex was not observed.[343-344] Rather, complete decarbonylation of the chromium complex takes place, and a hexacoordinated Cr complex is formed with the attachment of three equivalents of pyridyl hydrazine ligands where it acts as a bidentate ligand. Oxidative decarbonylation from metal carbonyl complexes using chelate ligands bearing acidic proton is reported in the literature.[345-346] In fact decarbonylation from a Cr(0) complex have been previously observed.[345]

Cr-1 was also investigated through UV-visible spectroscopy, showing absorption maxima at 291 nm in methanol at room temperature. The TDFT calculation of **L-1** showed this maximum at 291 nm corresponding to HOMO -4 to LUMO +2 [i.e., singlet ligand centred (Π - Π^*)] (around 89%) transitions. The complex displayed another absorption peak at 494 nm, which was attributed to the HOMO→L+8 (94%) as revealed by the DFT calculations. To, our delight complex displayed an absorption at 1004 nm in NIR region II, which is a rare phenomenon in case 3d transition metals, which is due to the H-1→LUMO (56%) and H-1→L+1 (14%) as predicted by DFT studied, our experimental data is in sync with the theoretically predicted data.

Excitingly the chromium complex displayed photoluminescent activity as well in NIR region II. Upon excitation with 530 nm, the complex displayed a peak at 1160 nm in emission spectra in solid state emission in NIR region II, which is rare in literature for 3d low valent transition metals. Cyclic voltammetry analysis reveals that **Cr-1** showed a reversible oxidation wave at -0.83V, as depicted in Figure 4.2. Investigation of the DFT calculated molecular orbitals showed that the HOMO is majorly localized on the chromium (0) centre with a minor contribution to the ligand backbone. Thus, it is confirmed that the oxidation of complex Cr-1 at potential -0.83V is associated with Cr(0)/Cr(I) oxidation, which is in line with the similar Cr(0) complexes.[345] The other peak at 1.28V appeared can be due to oxidation of the ligand motif. The structural parameters calculated from DFT are also closely matched with crystallography data. Selected bond angles and bond lengths are given in Table 4.3, along with the optimized structure of complex **Cr-1**.

Selected bond angles and bond lengths are given in Table 4.2.

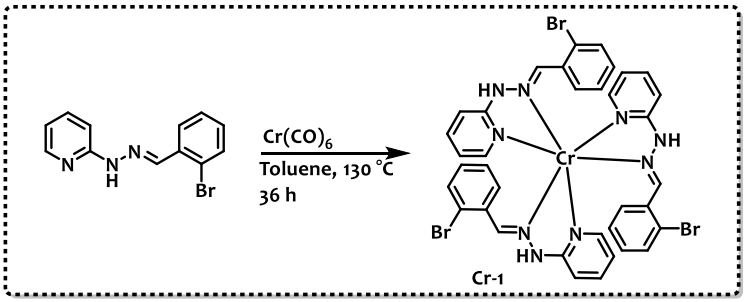

Scheme 4.1 Scheme for Complex Cr-1 synthesis.

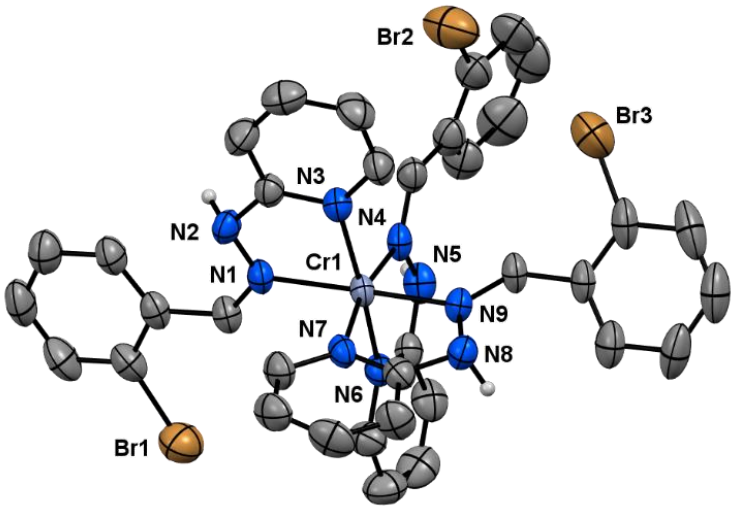

Fig. 4.1 ORTEP representation with partial atom labelling of complex **Cr-1** in 50% thermal ellipsoid probability. (Hydrogen atoms are omitted for clarity).

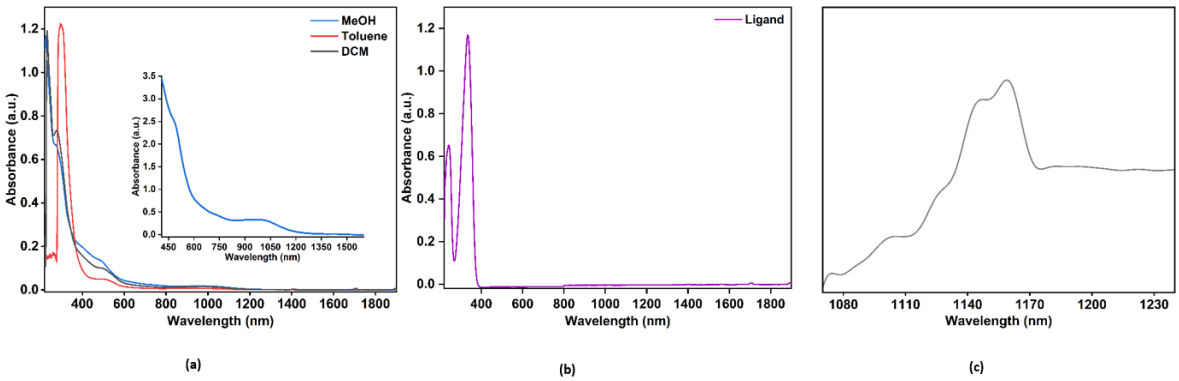

Fig. 4.2 (a) UV-Vis-NIR spectra of **Cr-1** complex. **(b)** UV-Vis-NIR spectra of ligand in dichloromethane. **(c)** Emission spectra of complex in solid state at room temperature.

4.2.1 In-vitro Biological Evaluation of Synthesized Cr-complex Cr-1

Being influenced by the literature showing the myriads of applications of the organometallic compounds, including antibacterial, antimalarial, and anticancer properties [347-348], we have tested the antimicrobial potential of the synthesized chromium-complex **Cr-1**. We first performed *in vitro* Kirby-Bauer agar diffusion experiments where we selected four pathogenic bacteria, including Gram-positive (*Bacillus subtilis* and *Staphylococcus aureus*) and Gram-negative (*Escherichia coli* and *Pseudomonas aeruginosa*). Our initial findings reveal that newly synthesized chromium-complex **Cr-1** can only kill positive bacteria, as is evident from the zone of inhibition on the LB agar plates compared to only DMSO (Figure 4.4 (A) upper panel). The diameter of the growth-inhibited zone is an indicator of antimicrobial potency, which we can observe for the respective bacteria *Bacillus subtilis* ~1.0 cm and *Staphylococcal aureus* ~0.9 cm. In the case of Gram-negative bacteria, there is no zone of inhibition that states moiety can specifically kill Gram-positive bacteria only but not Gram-negative ones. The reason behind the Gram-positive specificity of chromium-complex **Cr-1** might be the complex outer membrane (complex lipopolysaccharide and lipids) in Gram-negative bacteria that renders either its binding to respective receptors or unable to penetrate the compound inside the Gram-negative bacterial cells. Additionally, we were interested in determining the strength of the bactericidal effect by calculating the fold reduction in colony forming unit (CFU) into chromium-complex ligand treated versus non-treated *S. aureus* through a very conventional antimicrobial testing spot assay method. (Figure 4.3(B) upper panel). All the experiments were performed in biological and technical replicates. We obtained 7.0 x 109 CFU/ml in the treated culture, whereas in the control culture, it was approximately 7.65 x 10^{10} CFU/ml. These results suggest that chromium-complex **Cr-1** causes approximately 11-fold bacterial cell death compared to only DMSO control (DMSO is used as a vehicle for chromium-complex. All the experiments were performed in biological and technical replicates. We obtained 7.0 x 109 CFU/ml in the treated culture, whereas in the control culture, it was approximately 7.65 x 10^{10} CFU/ml. These results suggest that chromium-complex [Cr-1] ligand causes approximately 11-fold bacterial cell death as compared to only DMSO control (DMSO is used as a vehicle for chromium-complex [Cr-1.]

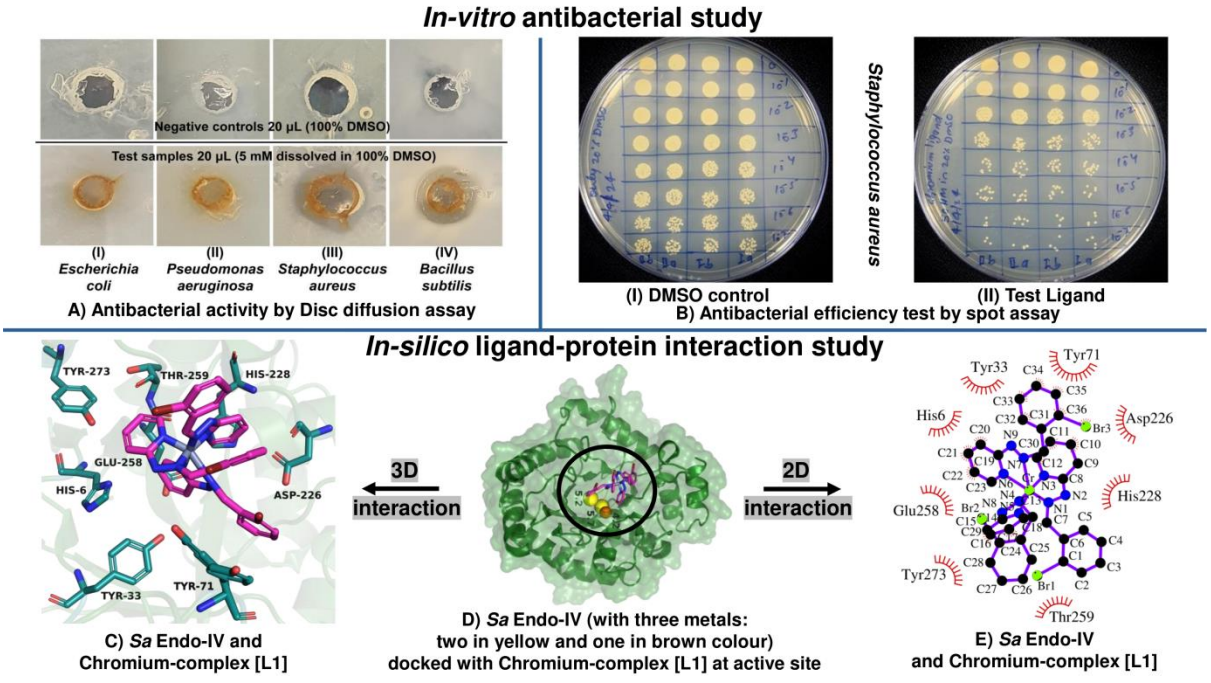

Fig. 4.3 Determination of antibacterial potential and probable molecular mode of action of chromium-complex [Cr-1] ligand upon binding to *S. aureus* DNA repair enzyme endonuclease-IV (*Sa* Endo-IV) active site.

The whole figure is divided into two-part upper parts (In vitro-based experiments) and a lower part (In silico pharmacophore-based therapeutic target screening). In the upper part, figure 4.4(A) indicates an agar diffusion test to screen the antibacterial potential of ligands against selected Gram-positive and Gram-negative bacteria. Similarly, figure 4.3(B) represents the spot assay to determine the efficiency of ligand on *S. aureus*, one of the Gram-positive bacteria. In the lower part we have shown the probable mechanism of bactericidal effect through *in silico* approaches. The centre figure in the lower panel (Figure 4.3(D) indicates S. aureus endonuclease-IV (PDB ID: 8AXY) with the docked conformation of the synthesized ligands chromium-complex. Figures on both sides of the centre figure in the lower part represent the 3D (Figure 4.3(C), left side) and 2D (Figure 4.3(E), right side) interaction profiles of the docked chromium-complex Cr-1 ligand **on *Sa* Endo-IV**. These two figures indicate that the conserved active site residues are involved in the protein-ligand interaction, and residues represented in spike (Figure 4.3(E) interact with hydrophobic bonding.

After getting the promising Gram-positive specific antibacterial outcomes from the in vitro results, we were interested in exploring the molecular mode of action of bactericidal effect on bacteria. One of the *in-silico* approaches that is based on the pharmacophore-guided potential drug target screening was applied herein. The preliminary sequels suggest that a possible binding partner of chromium-complex Cr-1 could be bacterial apurinic/apyrimidinic endonuclease (endonuclease-IV), a major DNA repair enzyme. This enzyme is present throughout the lower order genera, including Gram-positive and Gram-negative bacteria, but not in the higher order organisms like mammals and thus is considered a potential drug target for antibacterial therapy due to its nonexistence in humans [349]. DNA damage occurs during the normal metabolism process and when pathogens are exposed to stressful environments like oxidative stress, antibiotic stress, etc. If these damages are not taken care of within time, they lead to arrest in biological processes like replication and transcription, which eventually cause bacterial cell deaths [350]. Oxidatively damaged DNA are majorly repaired by two pathways, base excision repair (BER) and nucleotide incision repair (NIR), and our potential target for chromium-complex ligand AP endonuclease presented in this work plays a crucial role in this pathway.[351] BER pathway starts from DNA glycosylase, which cleaves the glycosidic linkage of the modified base, resulting in the apurinic/apyrimidinic (abasic) site working as a substrate for AP endonuclease which cleaves phosphodiester linkage at 5′ of abasic site producing 3′ free OH group. This class of enzyme also exhibits 5′ phosphodiesterase activity in the NIR DNA repair pathway and 3′-5′ exonuclease activity.352Multiple AP endonucleases are found in bacteria and humans, which are classified into two categories named exonuclease-III and endonuclease-IVs (Nfo). These endonucleases are metal-dependent nucleases like exonuclease-III, which needs Mg^{2+} for its catalytic activity, while endonuclease IV works in the presence of several metals like Mn^{2+} and Zn^{2+}.[353] *S. aureus* AP endonuclease requires three metal ions for its catalytic activity, and the following are the residues that are involved in the coordination of the metals His68, His109, Glu144, His181, Asp226, His228, Asp178, His213 and Glu258. The most important residue, Glu258, is directly involved in the final catalysis as it activates the water molecules for DNA strand cleavage.

Table 4.1 *In silico-based* molecular docking and deep learning-based affinity prediction of chromium-complex Cr-1 with the targeted *Sa* Endo-IV.

S.No.	Name of protein	Binding free energy (Kcal/Mol)	Affinity [pKd(-logKd]
1	Endonuclease-IV (S. aureus)	-11.3	7.68

Interestingly, in *S. aureus*, only one AP endonuclease endonuclease-IV type (Sa Endo-IV) exists, which contributes a major role in DNA repair. Hence inhibition of staphylococcal AP endonuclease is lethal for S. aureus; thus, it can be considered a potential drug target for Gram-positive specific antibacterial therapy.[354-355] The specificity of chromium-complex **Cr-1** towards Gram-positive bacteria and the non-availability of the Endonuclease-IV class of AP endonuclease in humans makes these promising antibacterial agents for future antibacterial drug discovery. Following the molecular target identification, blind molecular docking results reveal that the synthesized chromium-complex **Cr-1** presented herein selectively interacts with the *S. aureus* AP endonuclease (*Sa* Endo-IV) at interface of dsDNA binding in the active site cleft (Figure 4.4(D) down panel in centre) with very high free energy of binding ($\Delta G_{binding}$) -11.3 Kcal/Mol chromium-complex In detail analysis of protein-ligand interaction of *Sa* Endo-IV with docked poses of complex **Cr-1** indicates the involvement of physiologically important amino acid residues residing at or near to the catalytic groove (Figure 4.4(C), 4.4(D) and 4.4(E) lower panel). Interestingly, these residues are involved in the binding and stabilization of incoming damaged DNA followed by cleavage of phosphodiester bonds at 5′ of abasic site in the BER pathway and similar activity in 3′-5′ exonuclease activity and NIR pathway of DNA repair. The major amino acid residues of *Sa* Endo-IV, His6, Tyr33, Tyr71, Asp226, His228, Glu258, Thr259 and Tye273 are directly involved in the hydrophobic type of interaction with complex **Cr-1** (Figure 4.4(C) & 4.4(D) lower panel). These are the residues found to play a crucial catalytic role in the catalytic activity of Sa Endo-IV and are also responsible for the binding and stabilization of oxidatively damaged substrate DNA at its binding surface[354-355]. Therefore, the interaction of complex Cr-1 with Sa Endo-IV inhibited the DNA repair mechanism by inhibiting the binding and stabilization of damaged incoming DNA substrate, which may further lead to mutation and, consequently, bacterial cell deaths. Further, to support the excellent free energy of binding, we extend our *in-silico* experiment to calculate binding affinity. One of the freely available online tools KDEEP, which we have employed for binding affinity calculation. Interestingly, our KDEEP results also support the binding energy, and we have a nanomolar range of binding affinity of 7.68 for *Sa* Endo-IV AP endonuclease. Our comprehensive *in silico* and *in vitro* experimentation-based findings described herein provide new insight into the antimicrobial lead molecule-like potential in the synthesized complex **Cr-1,** which shows a narrow range of antibacterial activity against Gram-positive bacteria and its exerted biological effects due to the interruption of DNA repair function of the physiologically vital dsDNA repair enzyme, AP endonuclease of the targeted organism. Detailed structure-function studies, pharmacokinetic profiling, and toxicity studies will ensure this scaffold's therapeutic efficacy and safety for future therapeutic uses.

4.3 Experimental Section

The complex **Cr-1** was prepared as per Scheme **4.1**.

Primarily, the ligand synthesis was carried out according to the literature procedure by adding the ethanolic solution of 2-pyridyl hydrazine to the ethanolic solution of 2-bromobenzaldehyde dropwise, a catalytic amount of acetic acid was added, after which imine formation started immediately. The resulting solution was stirred for an hour at room temperature. Afterwards, the reaction was stopped, and the white precipitates thus obtained were collected and dried under a vacuum.[342] Afterwards, 73 mg of $Cr(CO)_6$ (0.33 mmol) was added to the 25 mL Schlenk flask already charged with a toluene solution of **L** 275 mg (1 mmol) inside the glove box. Schlenk was removed from the glove box and heated to 130°C over a pre-heated oil bath. Afterwards, the reaction was stopped and allowed to cool up to room temperature. The reddish-brown solution thus obtained was dried under a vacuum and washed twice with pentane. Single crystals suitable for diffraction were obtained in saturated methanol solution using a slow evaporation technique.

4.3.1. Representative Characterization Data for Complex Cr-1

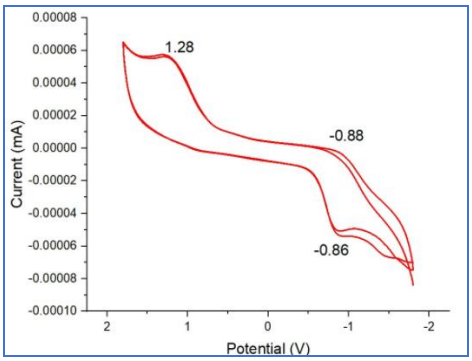

Fig.4.4 CV of **Cr-1**. Conditions: 1.0 mM analyte in 0.1 M TBAPF6/DMF, under dry argon atmosphere, glassy carbon working electrode, platinum wire counter electrode, $Ag/AgNO_3$ reference electrode.

HRMS Data Expected mass – 876.9579, Found- 876.9412.

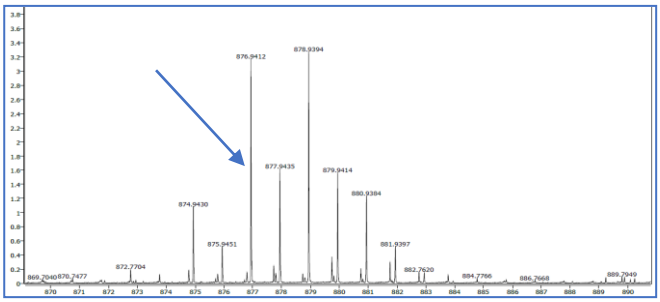

Fig.4.5 HRMS data for the complex **Cr-1**

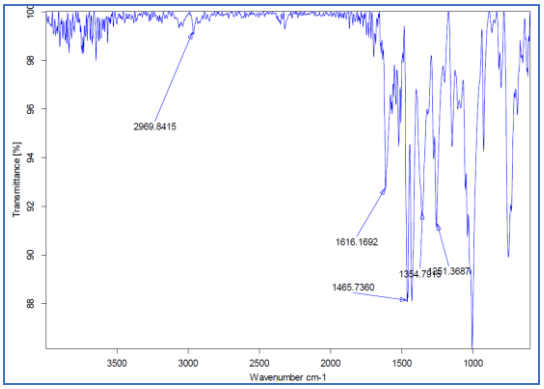

Fig.4.6 IR Spectra of the complex **Cr-1**

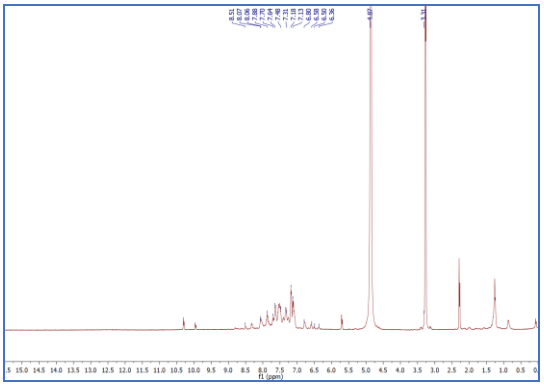

Fig. 4.7 ^1H NMR for the complex **Cr-1** in CD3OD

All calculations were performed with the Gaussian16 employing the DFT method, the Becke three-parameter hybrid functional, and Lee-Yang-Parr's gradient-corrected correlation functional (B3LYP). Singlet ground state geometry optimization for complex **Cr-1** was carried out at the (R)B3LYP level in the gas phase, using its respective .cif files. All elements except Cr(0) were assigned the 6-31G(d,f) basis set. The double-ζ quality SBKJC-VDZ basis set with an effective core potential was employed for the Cr(0) atom. Vertical electronic excitations based on (R)B3LYP S4 optimized geometries were computed for R1, 1 and R2 using the TD-DFT formalism in methanol. Vibrational frequency calculations were performed to ensure that the optimized geometries represent the local minima and there are only positive eigenvalues. The electronic distribution and localization of the singlet excited states were visualized using the electron density difference maps (ED-DMs). Gausssum 2.2 was employed to visualize the absorption spectra (simulated with Gaussian distribution with a full-width at half maximum (fwhm) set to 3000 cm-1) and to calculate the fractional contributions of various groups to each molecular orbital. All calculated structures were visualized with ChemCraft and analyzed with Chemissian.[356-360]

Table 4.2 Crystal data and structure refinement for **Cr-1.**

Identification code		**Cr-1**
CCDC No.		2346716
Empirical formula		$C_{36}H_{30}Br_3CrN_9$
Formula weight		880.42
Temperature/K		273(2)
Crystal system		triclinic
Space group		P-1
a/Å		8.821(3)
b/Å		10.589(3)
c/Å		19.583(6)
α/°		97.701(9)
β/°		94.433(11)
γ/°		103.279(10)
Volume/Å3		1753.1(9)
Z		2
ρcalcg/cm3		1.668
μ/mm-1		3.786
F(000)		876.0
Radiation		Mo Kα (λ = 0.71073)
2Θ range for data collection/°		4.774 to 50.24

Reflections collected		31007
Independent reflections		6210 [Rint = 0.1112, Rsigma = 0.0853]
Data/restraints/parameters		6210/9/451
Goodness-of-fit on F2		1.032
Final R indexes [I>=2σ (I)]		R1 = 0.0641, wR2 = 0.1855
Final R indexes [all data]		R1 = 0.1014, wR2 = 0.2084
Largest diff. peak/hole / e Å-3		0.99/-0.92

Table 4.3 Selected experimental and calculated (DFT) bond lengths (Å) and bond angles (°) of the complex **Cr-1**

Bonds Lengths (Å)	**Complex, Cr-1**		**Bonds Angles (°)**	**Complex, Cr-1**	
	X-ray	**DFT**		**X-ray**	**DFT**
Br1-C1	1.914(7)	1.9301	N1-Cr1-N4	95.12(18)	94.7428
Br2-C15	1.905(8)	1.9301	N1-Cr1-N9	170.01(18)	170.0394
Br3-C36	1.876(8)	1.9288	N3-Cr1-N1	77.46(19)	78.9973
Cr1-N1	2.058(5)	2.0543	N3-Cr1-N4	97.25(19)	93.7627
Cr1-N3	2.033(5)	2.0140	N3-Cr1-N9	97.09(18)	95.4209
Cr1-N4	2.064(5)	2.0603	N4-Cr1-N9	93.86(18)	93.8472
Cr1-N6	2.030(5)	2.0102	N6-Cr1-N1	96.53(19)	93.1885
Cr1-N7	2.018(5)	1.9998	N6-Cr1-N3	171.63(19)	169.8162
Cr1-N9	2.068(4)	2.0624	N6-Cr1-N4	77.31(19)	78.8556
N1-N2	1.360(7)	1.3869	N6-Cr1-N9	89.69(18)	93.81134
N1-C7	1.311(7)	1.3334	N7-Cr1-N1	94.20(18)	93.9925
N2-C8	1.344(7)	1.3758	N7-Cr1-N3	91.71(18)	92.4994
N3-C8	1.360(7)	1.3577	N7-Cr1-N4	168.27(18)	169.9439
N3-C12	1.362(8)	1.3609	N7-Cr1-N6	94.56(19)	94.0407
N4-N5	1.351(7)	1.3840	N7-Cr1-N9	77.47(18)	79.3002
N4-C13	1.327(8)	1.3353	N2-N1-Cr1	116.3(3)	113.8831
N5-C20	1.364(8)	1.3789	C7-N1-Cr1	123.9(4)	129.9692
N6-C20	1.342(7)	1.3588	C8-N3-Cr1	112.3(4)	114.1128
N6-C24	1.386(8)	1.3562	C12-N3-Cr1	128.3(4)	129.1134
N7-C25	1.380(7)	1.3561	N5-N4-Cr1	116.0(4)	113.7595
N7-C29	1.342(8)	1.3599	C13-N4-Cr1	123.6(4)	129.5397
N8-N9	1.360(7)	1.3840	C20-N6-Cr1	113.7(4)	114.7996
N8-C29	1.349(7)	1.3767	C24-N6-Cr1	127.8(4)	128.4621
N9-C30	1.299(7)	1.3284	C25-N7-Cr1	128.8(4)	128.7913
			C29-N7-Cr1	112.8(4)	114.6024
			N8-N9-Cr1	115.6(3)	113.1918
			C30-N9-Cr1	126.4(4)	129.8126

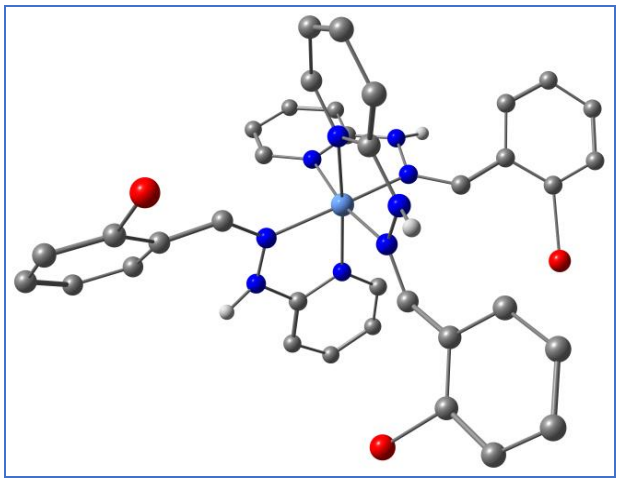

Fig. 4.8 Optimized structure of the complex **Cr-1**

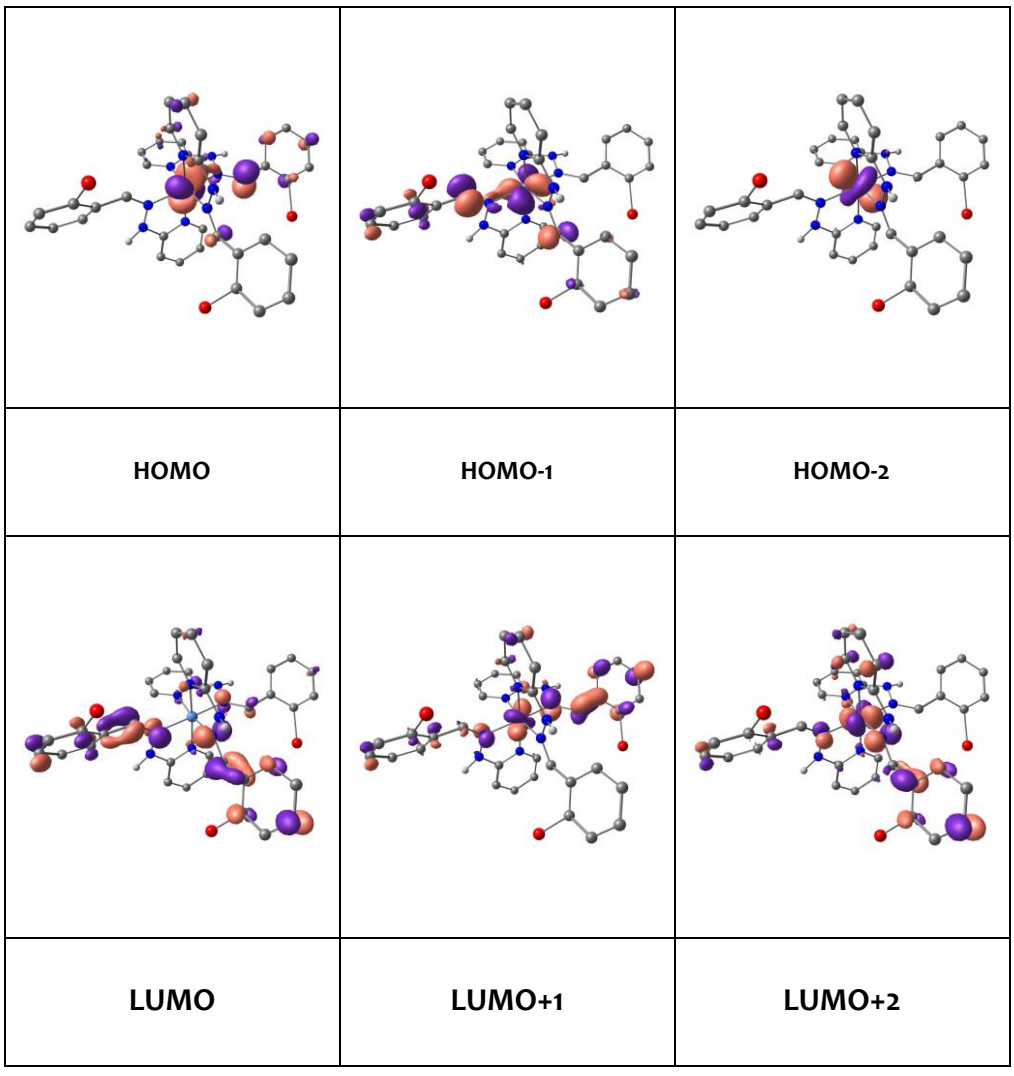

Fig. 4.9 Molecular orbitals of complex, **Cr-1** (isosurface value= 0.05).

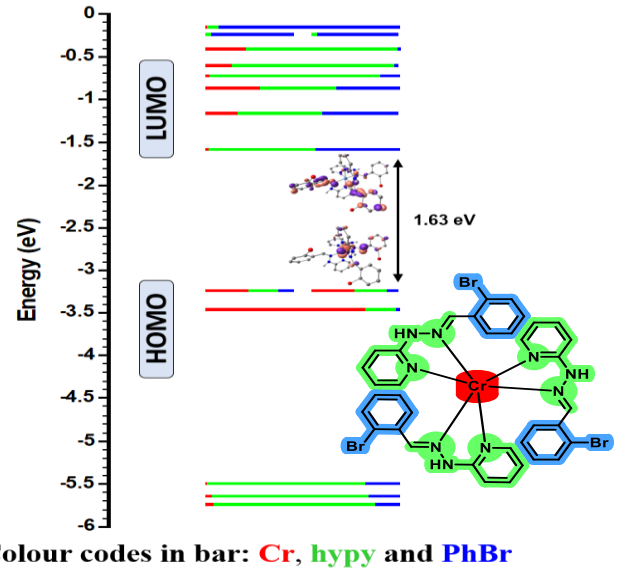

Fig. 4.10 Calculated frontier MO energies of **Cr-1** calculated from DFT [B3LYP/SBKJC-VDZ for Cr(0) and 6-31g** for C, H, N, Br] and 0.05 eV threshold of degeneracy. Kohn-Sham MOs of HOMO and LUMO are also shown.

Table 4.4 Selected Transitions from TD-DFT calculations of **Cr-1** in the Singlet Ground State (B3LYP/ SBKJC-VDZ for Cr(0) and 6-31G** for [C, H, N, Br] (MeOH)).

λabs/nm (TD-DFT)	λabs/nm [expt.]	f (TD-DFT)	Major transition(s)	Character
304	291	0.0894	H-4→L+2 (89%)	hypy(π)→hypy(π*) (major), hypy(π)→PhBr(π*) (major)
504	494	0.0115	HOMO→L+8 (94%)	Cr(dπ)→PhBr(π*) (major) hypy(π)→PhBr(π*) (major)
951	1004	0.3203	H-1→LUMO (56%) H-1→L+1 (14%)	Cr(dπ)→PhBr(π*) (minor) Cr(dπ)→hypy(π*) (minor) hypy(π)→PhBr(π*) (minor) hypy(π)→hypy(π*) (minor) PhBr(π)→PhBr(π*) (minor) PhBr(π)→hypy(π*) (minor)

4.3.2 In-vitro Assessment of Antibacterial Potential

In view of the biological relevance of the synthesized organometallic complex, we examine the antibacterial potential against a wide range of Gram-positive and Gram-negative bacteria. We have performed the agar diffusion test to assess the antibacterial potential against representative genera of Gram-positive and Gram-negative bacteria, including *Bacillus subtilis, Staphylococcus aureus*, *Escherichia coli* and *Pseudomonas aeruginosa*. In brief, log-phase bacterial cultures (optical density approximately 0.6) were spread on LB agar and then incubated at 37°C for 30 min. The ligand chromium-complex [Cr-1] (5 mM) 20 µl solutions in 100% DMSO were inundated in wells on the agar plate alongside an identical volume of 100% DMSO as a control to negate its effect. The plates were incubated at 37°C overnight to develop a clear zone of inhibition. Subsequently, post overnight incubation, the clear zone of inhibition surrounding the wells indicates the bactericidal potential as a function of radial diffusion of ligand chromium-complex [L1] ligand or the control (100 % DMSO) solutions were recorded. Additionally, we have performed the spot assay of chromium-complex Cr-1 ligand against *S. aureus* by serial 10-fold dilution and spots on the agar plates. Again, the log phase culture of *S. aureus* was treated with 50 µM of the chromium-complex Cr-1 ligand and with an identical volume of 100% DMSO as a negative control for 2 h at 37°C. The cultures were serially 10-fold diluted till 10^{-7} fold

dilution, followed by spotting 5 µl of the diluted cultures on the agar plates. All the plates were incubated overnight at 37°C. Post completion of incubation colonies were calculated on each plate and compared with the control to determine the fold reduction in the number of colonies forming units upon treatment with chromium-complex Cr-1 ligand compared to only DMSO treatment.[361-362]

4.3.3 In-silico Pharmacophore Guided Biological Target Screening of Cr-complex Cr-1

The crystal structure of the chromium-complex Cr-1 ligand bestowed the pharmacophoric information of the synthesized ligand. Thus, derived pharmacophore information was harnessed to screen the persuasive biological target of the synthesized chromium-complex Cr-1 ligand through an in silico reverse docking approach using a therapeutic target database. The Initial outcomes of reverse docking indicate that AP endonuclease could be a potential therapeutic target of this synthesized ligand. To validate the initial findings, we employed an in-silico application based on the Lamarkian Genetic Algorithm called Autodock vina that can be used to perform receptor-based one-to-one molecular docking of ligands and receptors. The 3-dimensional crystal structure of staphylococcal AP endonuclease (Sa Endo-IV) belonging to one of the Gram-positive bacteria Staphylococcus aureus was retrieved from an online repository protein data bank (PDB ID:8AXY). Subsequently, the water molecules, associated ligands, and other remaining non-bonded and non-protein molecules, except metal ions, were expunged with the help of PyMol. In order to prepare receptor molecules for molecular docking, polar hydrogen and Kollman charges were incorporated into the receptor protomer with the help of molecular graphic laboratory tools (MGL Tools). MGL Tools are also employed to prepare ligands and fix the number of rotatable bonds. In the view of whole protein as a target for ligand accessibility, the blind docking approach was taken into consideration for chromium-complex [Cr-1] ligand with the aforementioned Sa Endo-IV. The grid box size for Sa Endo-IV was kept 52ÅX60ÅX56Å with 1Å of the grid spacing. Although Autodock Vina provides nine plausible poses where our ligand of interest could interact, we take the most favourable pose as it has the lowest root mean square deviation (RMSD) value and lowest free energy of binding (ΔGBinding). Further interaction profile of the chromium-complex [Cr-1] ligand with Sa Endo-IV was investigated and compared with E.coli Nfo solved crystal structure (PDB ID:2NQ9) by utilizing PyMol and LigPlot. The binding affinity of receptor and ligand provides a glimpse of the strength of binding partners, so we have calculated the binding affinity of the chromium-complex [Cr-1] ligand with Sa Endo-IV. One deep learning-based online tool, KDEEP, was employed for affinity predictions.[363-368]